Microsystem Technologies 9 (2003) 474–479 © Springer-Verlag 2003
DOI 10.1007/s00542-002-0277-4

Modal analysis of a unimorph piezoelectrical transducer

C. Liu, T. Cui, Z. Zhou

Abstract Piezoelectric transducers are widely applied to MEMS devices as actuators or sensors due to their simple structure and easy control. A micromachined piezoelectric microjet is introduced and modal analysis of its piezoelectric actuator has been thoroughly presented. Both numerical analysis and experimental measurement are implemented in this study. In numerical analysis, an approximate method is established to evaluate the first vibration mode and finite-element methods are used to simulate higher order vibration modes of the transducer. An experimental system was also set up to measure the axisymmetric vibration modes of the transducer. Compared with experimental results, good correlation was found between the numerical and experimental results, which proved the validation and reliability of the models. Through these models, further optimal design of the transducer can be carried out.

List of symbols

a	the radius of elastic plate
b	the radius of piezoelectric disk
d_{31}	piezoelectric coupling coefficient
D_z	electric displacement along z direction
E_1	the Young's modulus of piezoelectric material
E_2	the Young's modulus of elastic plate
E_z	the electric field
g_{31}	piezoelectric strain constant
h_1	thickness of piezoelectric disk plus half of elastic plate
$2h_2$	thickness of elastic plate
$\bar{m}_1$	mass density of piezoelectric disk per unit area
$\bar{m}_2$	mass density of elastic plate per unit area
S_i	$i = 1, 2$ strains along r and θ directions
T_i	$i = 1, 2$ stresses along r and θ directions
w	the transverse deflection of the transducer
$W(r)$	the mode shape function of the transducer
σ_1	the Poisson's ratio of the piezoelectric material
σ_2	the Poisson's ratio of the elastic plate
α	rate of radii of piezoelectric disk to the elastic plate
β	rate of thickness of the elastic plate to piezoelectric disk
β_{33}^{T}	coefficient of dielectric impermeability
ω	radian frequency of the driving signal

Received: 14 May 2002/Accepted: 28 June 2002

C. Liu, T. Cui (✉)
Institute For Micromanufacturing (IFM),
Louisiana Tech University, Ruston, LA 71272, USA
E-mail: tcui@coes.latech.edu

Z. Zhou
Department of Precision Instruments,
Tsinghua University, Beijing 100084, China

Financial support by National Natural Science Funds (29833070) and National 973 Basic Research Projects (G1999033106) of China is deeply appreciated.

1 Introduction

Compared to multi-layer and bimorph piezoelectric transducers, the unimorph piezoelectric transducer is also in wide use for its simple structure and easy assembly, especially in microfluidics control and delivery. Among the unimorph piezoelectric transducers, some transducers work at far below the first resonant frequency, such as piezoelectric micropumps [1]. Some transducers work at the first vibration mode, such as some ultrasonic liquid ejectors [2]. Moreover, some piezoelectric transducers work at higher order vibration modes, such as some microfluidics sprayers [3] for DNA mass spectrometry. New applications of unimorph piezoelectric transducers are still emerging.

A piezoelectric microjet based on the basic principle of Drop-On-Demand ink-jets, has recently been developed [4, 5]. The device consists of a fluid chamber, which is formed by a piezoelectric unimorph transducer bonded to a silicon chip with nozzle arrays as shown in Fig. 1. By micromachining techniques, 640 nozzles, 5 μm in diameter, are fabricated through membranes 15 μm thick etched by KOH on a silicon chip 3.5 mm by 3.5 mm. A piezoelectric disk, 9 mm in diameter and 0.4 mm thick, is glued to another silicon chip, which is first etched to form an elastic membrane 10 mm in diameter and 100 μm thick, constituting the unimorph piezoelectric transducer.

Driven by an electrical pulse at certain frequencies, the piezoelectric transducer generates a pressure wave, which propagates towards the nozzles in the fluid chamber and squeezes the liquid out. With enough kinetic energy, the liquid releases through the nozzles and forms droplets. The piezoelectric microjet works at its resonant frequencies and, if vibrating in its higher mode, will obtain higher kinetic energy and flow rate. Therefore, it is necessary for the device to work at higher resonant frequencies to meet the application requirements. A microjet is in ejection of liquid droplets, as illustrated in Fig. 2.

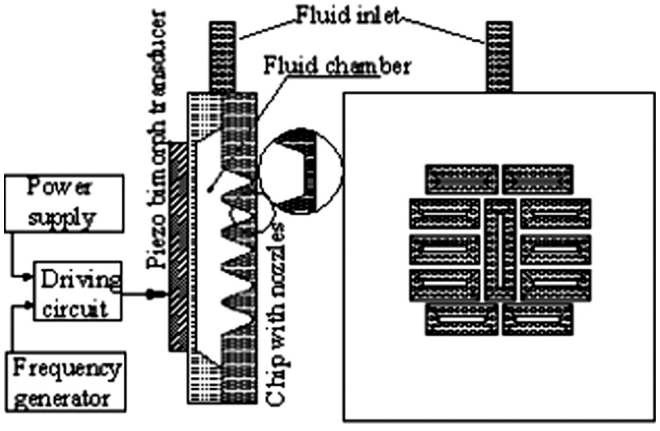

Fig. 1. Structure of a microjet and its driving system

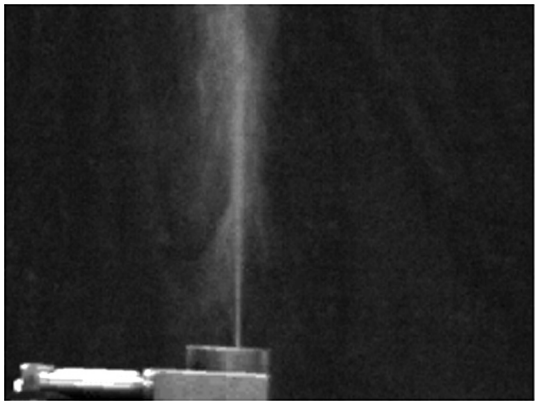

Fig. 2. A microjet in ejection of liquid droplets

Until now, however, research work has mainly focused on experimentation, fabrication and processing of piezoelectric transducers. Only a few simple analytical [5, 6] and numerical models [7, 8] have been reported on piezoelectrical transducers, especially the piezoelectric unimorph transducer. Fewer investigations are focused on modal analysis of the transducer. Based on the experimental results of the micromachined devices, this paper successfully establishes an approximate method for evaluating the first vibration mode, and the finite-element method is used to simulate the higher order axisymmetric vibration modes. Comparisons with experimental results prove the validation of the models. Through these models presented in this paper, further optimal design of the transducer is ready to carry out.

2
Approximate calculation of basic mode

Most unimorph piezoelectric transducers work at or below the first resonant frequency, therefore thorough understanding of the first vibration mode of transducers is necessary.

By simplifying the transducer as a silicon-piezoelectric bonded structure, the model of the transducer illustrated in Fig. 3 consists of a circular elastic plate with the edge clamped and a piezoelectric disk bonded concentrically.

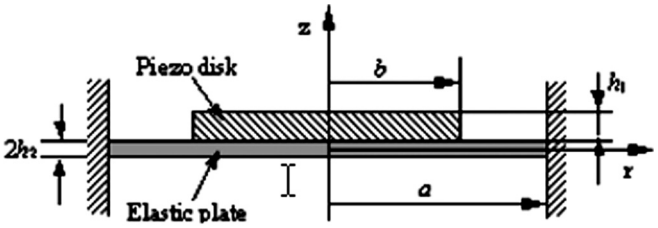

Fig. 3. Model of a silicon-piezoelectric unimorph transducer

2.1
Displacement mode shape function

The following conditions are assumed:

(1) The displacement of the transducer is small enough and all the materials are in their linear elastic range.
(2) Each layer is continuous along the thickness direction, that is, the transverse deflection is the same along z direction.
(3) There are no shear strains and only the flexural vibration is considered.
(4) The piezoelectric layer is polarized along z direction and the thickness is thin enough so that the electric field is only along z direction and keeps constant.

According to the above assumptions, the bending theory of thin plates is applicable. When the transducer vibrates in its axisymmetric modes, the general expression for the transverse displacement $w(r,t)$ is

$$w(r,t) = A \cdot W(r) \cdot \mathrm{e}^{\mathrm{j}\omega t} \tag{1}$$

Subject to certain approximations, the first mode shape function $W(r)$ can be expanded with a polynomial expression as

$$W(r) = 1 + a_2\left(\frac{r}{a}\right)^2 + a_3\left(\frac{r}{a}\right)^3 + a_4\left(\frac{r}{a}\right)^4 \tag{2}$$

Assuming $\zeta = A\mathrm{e}^{\mathrm{j}\omega t}$, $\xi = \dot{\zeta} = \zeta j\omega$, thus

$$\dot{w}(r,t) = W(r) \cdot \xi \tag{3}$$

2.2
Kinetic and potential energies

The total kinetic energy of the transducer is composed of the kinetic energy of the elastic plate and the kinetic energy of the piezoelectric disk [9]. The kinetic energy of the elastic plate can be given by

$$T_S = \frac{1}{2}\int_0^a \int_{-h_2}^{h_2} \rho_2 \dot{w}^2(r,t)\cdot 2\pi r \,\mathrm{d}r\,\mathrm{d}z \tag{4}$$

Combining Eqs. (3) and (4), thus

$$T_S = \frac{\bar{m}_2}{2}\pi a^2 \xi^2 K_S \tag{5}$$

where

$$K_S = 1 + a_2 + \tfrac{4}{5}a_3 + \tfrac{2}{3}a_4 + \tfrac{1}{3}a_2^2 + \tfrac{1}{4}a_3^2 + \tfrac{1}{5}a_4^2 + \tfrac{4}{7}a_2a_3 + \tfrac{4}{9}a_3a_4 + \tfrac{1}{2}a_2a_4 \tag{6}$$

As the same way, the kinetic energy of the piezoelectric disk can be given by

$$T_P = \frac{\bar{m}_1}{2}\pi b^2 \xi^2 K_P \tag{7}$$

where

$$K_P = 1 + a_2\alpha^2 + \tfrac{4}{5}a_3\alpha^3 + \tfrac{2}{3}a_4\alpha^4 + \tfrac{1}{3}a_2^2\alpha^4 + \tfrac{4}{7}a_2a_3\alpha^5 + \tfrac{1}{2}a_2a_4\alpha^6 + \tfrac{1}{4}a_3^2\alpha^6 + \tfrac{4}{9}a_3a_4\alpha^7 + \tfrac{1}{5}a_4\alpha^8 \tag{8}$$

Thus, the total kinetic energy of the transducer is

$$T_T = T_P + T_S = \frac{\bar{m}_1}{2}\pi b^2 \xi^2 K_P + \frac{\bar{m}_2}{2}\pi a^2 \xi^2 K_S \tag{9}$$

The total potential energy is also composed of two parts, the potential energy of the elastic plate and the piezoelectric disk. According to the bending theory of thin plates, the stresses of the elastic plate are

$$T_1 = \frac{E_2}{1-\sigma_2^2}(S_1 + \sigma_2 S_2) \tag{10a}$$

$$T_2 = \frac{E_2}{1-\sigma_2^2}(S_2 + \sigma_2 S_1) \tag{10b}$$

where $S_1 = -z \cdot \mathrm{d}^2w/\mathrm{d}r^2$, $S_2 = -(z/r) \cdot \mathrm{d}w/\mathrm{d}r$. Therefore, the potential energy of the elastic plate is

$$U_S = \int_0^a \int_{-h_2}^{h_2} \tfrac{1}{2}(T_1S_1 + T_2S_2) \cdot 2\pi r \, \mathrm{d}r \, \mathrm{d}z \tag{11}$$

Substituting Eq. (10) into Eq. (11) yields

$$U_S = \frac{2\pi E_2 h_2^3 \zeta^2}{3(1-\sigma_2^2)a^2}\Lambda_S \tag{12}$$

where

$$\Lambda_S = 4(1+\sigma_2)a_2^2 + 12(1+\sigma_2)a_2a_3 + (\tfrac{45}{4} + 9\sigma_2)a_3^2 + 16(1+\sigma_2)a_2a_4 + \left(\tfrac{168}{5} + 24\sigma_2\right)a_3a_4 + \left(\tfrac{80}{3} + 16\sigma_2\right)a_4^2 \tag{13}$$

According to the electromechanical coupling mechanisms in the transducer, thus

$$T_1 = \frac{E_1}{1-\sigma_1^2}(S_1 + \sigma_1 S_2) - \frac{g_{31}E_1}{1-\sigma_1}D_z \tag{14a}$$

$$T_2 = \frac{E_1}{1-\sigma_1^2}(S_2 + \sigma_1 S_1) - \frac{g_{31}E_1}{1-\sigma_1}D_z \tag{14b}$$

$$E_z = \beta_{33}^T D_z - g_{31}(T_1 + T_2) \tag{14c}$$

Integrating the two sides of Eq. (14c) along the axial direction of the piezoelectric disk, therefore the driving voltage V_z results from

$$V_z = \int_{h_2}^{h_1+h_2} E_z \, \mathrm{d}z = \beta_{33}^E h_1 D_z - \frac{E_1 g_{31} h_1^2(1+\beta)}{2(1-\sigma_1)}\left(\frac{\mathrm{d}^2w}{\mathrm{d}r^2} + \frac{1}{r}\frac{\mathrm{d}w}{\mathrm{d}r}\right) \tag{15}$$

Assuming $V_z = 0$, the electric displacement with a constant voltage is given by

$$D_z = \frac{E_1 g_{31} h_1(1+\beta)}{2\beta_{33}^E(1-\sigma_1)}\left(\frac{\mathrm{d}^2w}{\mathrm{d}r^2} + \frac{1}{r}\frac{\mathrm{d}w}{\mathrm{d}r}\right) \tag{16}$$

where

$$\beta_{33}^E = \beta_{33}^T + \frac{2E_1 g_{31}^2}{1-\sigma_1} \tag{17}$$

Thus, the potential energy of the piezoelectric disk is

$$U_P = \int_0^a \int_{h_2}^{h_1+h_2} \tfrac{1}{2}(T_1S_1 + T_2S_2) \cdot 2\pi r \, \mathrm{d}r \, \mathrm{d}z \tag{18}$$

Substituting Eqs. (14) and (16) into Eq. (18) yields

$$U_P = \frac{2\pi E_1 \varphi h_1^3 \zeta^2}{3(1-\sigma_1^2)a^2}\Lambda_P^D - \frac{\pi E_1^2 g_{31}^2 h_1^3 \zeta^2 (1+\beta)^2}{2\beta_{33}^E(1-\sigma_1)^2 a^2}\Lambda_P^V \tag{19}$$

where

$$\varphi = 1 + \tfrac{3}{2}\beta + \tfrac{3}{4}\beta^2, \tag{20a}$$

$$\Lambda_P^D = 2(1+\sigma_1)a_2^2\alpha^2 + 6(1+\sigma_1)a_2a_3\alpha^3 + \left(\tfrac{45}{8} + \tfrac{9}{2}\sigma_1\right)a_3^2\alpha^4 + 8(1+\sigma_1)a_2a_4\alpha^4 + \left(\tfrac{84}{5} + 12\sigma_1\right)a_3a_4\alpha^5 + \left(\tfrac{40}{3} + 8\sigma_1\right)a_4^2\alpha^6, \tag{20b}$$

$$\Lambda_P^V = 4a_2^2\alpha^2 + 12_2a_3\alpha^3 + \tfrac{81}{8}a_3^2\alpha^4 + 16a_2a_4\alpha^4 + \tfrac{144}{5}a_3a_4\alpha^5 + \tfrac{64}{3}a_4^2\alpha^6 \tag{20c}$$

Therefore, the total potential energy of the piezoelectric transducer is

$$U_T = U_P + U_S = \frac{2\pi E_1 \varphi h_1^3 \zeta^2}{3(1-\sigma_1^2)a^2}\Lambda_P^D - \frac{\pi E_1^2 g_{31}^2 h_1^3 \zeta^2 (1+\beta)^2}{2\beta_{33}^E(1-\sigma_1)^2 a^2}\Lambda_P^V + \frac{2\pi E_2 h_2^3 \zeta^2}{3(1-\sigma_2^2)a^2}\Lambda_S \tag{21}$$

2.3 Energy method

Due to the boundary situation of clamped edge, the relationship of the parameters is given as

$$a_3 = -4 - 2a_2, \quad a_4 = 3 + a_2 \ . \tag{22}$$

According to the conservation principle of total momentum of the system, equating the maximum potential and kinetic energies of the transducer yields

$$U_T^{\max} = T_T^{\max} \tag{23}$$

That is

$$\frac{2\pi E_1 \varphi h_1^3 \zeta^2}{3(1-\sigma_1^2)a^2}\Lambda_P^D - \frac{\pi E_1^2 g_{31}^2 h_1^3 \zeta^2 (1+\beta)^2}{2\beta_{33}^E(1-\sigma_1)^2 a^2}\Lambda_P^V + \frac{2\pi E_2 h_2^3 \zeta^2}{3(1-\sigma_2^2)a^2}\Lambda_S = \frac{\overline{m}_1}{2}\pi b^2 \omega^2 K_P + \frac{\overline{m}_2}{2}\pi a^2 \omega^2 K_S \tag{24}$$

Equation (24) can also be written as

$$\omega^2 = \frac{c_1\Lambda_P^D - c_2\Lambda_P^V + c_3\Lambda_S}{c_4K_P + c_5K_S} \tag{25}$$

where

$$c_1 = \frac{2\pi E_1 \varphi h_1^3}{3(1-\sigma_1^2)a^2}, \quad c_2 = \frac{\pi E_1^2 g_{31}^2 h_1^3 (1+\beta)^2}{2\beta_{33}^E (1-\sigma_1)^2 a^2},$$

$$c_3 = \frac{2\pi E_2 h_2^3}{3(1-\sigma_2^2)a^2}, \quad c_4 = \frac{\overline{m}_1}{2}\pi b^2, \quad c_5 = \frac{\overline{m}_2}{2}\pi a^2 \qquad (26)$$

Substituting Eq. (22) into Eq. (25), ω is then a function of a_2. By the application of the energy method, a_2 can be determined as

$$\frac{\mathrm{d}(\omega^2)}{\mathrm{d}a_2} = 0 \qquad (27)$$

Combining Eqs. (25) and (27), a_2 is ready to be solved. Thus, a_3, a_4 and the first frequency ω can be obtained.

For most piezoelectric transducers, such as piezoelectric micropumps and some piezoelectric actuators for precision motion, working at far below first frequency or just at the first vibration mode, the approximate calculation of the first mode can meet requirements of most engineering applications. However, it is not enough for some other piezoelectric transducers, such as piezoelectric microjets. As mentioned above, they should work at higher frequencies to get high enough kinetic energy to release tiny droplets from nozzles and to obtain a high enough flow. Therefore, the finite-element method has been utilized for higher order vibration modes analysis of the transducer. In addition, all the numerical results of the first mode and higher order modes will be compared to the experimental results.

3
Finite-element method for modal analysis

The above approximate method for the first mode only considered the circular chamber part of the transducer and assumed the circumferential edge clamped. However, as shown in Fig. 1, the total transducer is square and the real boundary conditions are the four rims clamped. For the complexity of the structure, the finite-element method (FEM) is used to simulate the higher order vibration modes of the transducer.

In this paper, FEM software, ANSYS, has been used to analyze the transducer. Only axisymmetric vibration modes will be concerned, one-fourth part of the device has been modeled as shown in Fig. 4. Here the elastic plate is a silicon chip 400 μm thick, and the chamber membrane is 10 mm in diameter and 100 μm thick. The piezoelectric disk, 10 mm in diameter and 0.4 mm thick, is bonded to the other side of the chamber membrane concentrically. The bonding layer is negligible. The driving voltage is set zero, that is, a short-circuit status of the piezoelectric disk.

Figure 6a shows the first three axisymmetric vibration mode shapes corresponding to the resonant frequencies at 21, 64, 155 kHz. It is found that only these axisymmetric modes, with no zero displacement at the center of the chamber membrane, result in the volume change of the chamber and the transducer can steadily work under these modes. The open-circuit status and non-piezoelectric phenomenon have been studied. Less than 1% difference of the results from the ones under the short-circuit status demonstrates that the electromechanical coupling is negligible in modal analysis, which will simplify the optimal design of the transducer and reduce the calculation work.

4
Comparisons with experimental results

An approximate method has been presented above to evaluate the approximate solution of the basic vibration mode of the transducer. Finite element analysis has also been used to simulate the higher order modes of the structure. However, due to the complexity of the device and many assumptions during modeling, experimental measurement is indispensable to testify the validity and reliability of numerical analysis.

4.1
Comparison of first mode results

Based on the approximate method introduced above, the first mode of the real device has been calculated and compared with the experimental results. Substituting the related parameters of the transducer yields $a_2 = -0.5683$, $a_3 = -2.8634$, and $a_4 = 2.4317$. Thus, the first mode shape function results from

$$W(r) = 1 - 0.5683\left(\frac{r}{a}\right)^2 - 2.8634\left(\frac{r}{a}\right)^3 + 2.4317\left(\frac{r}{a}\right)^4 \qquad (28)$$

Figure 5 illustrates the calculated and experimental results of the first mode shape function along the diameter of the transducer. The calculated first frequency is 36 kHz, while the measured result is 28.1 kHz. From the comparisons, it is easily found that there are obvious differences between the calculated mode shape and the experimental result near the edges, and the calculated frequency and measured

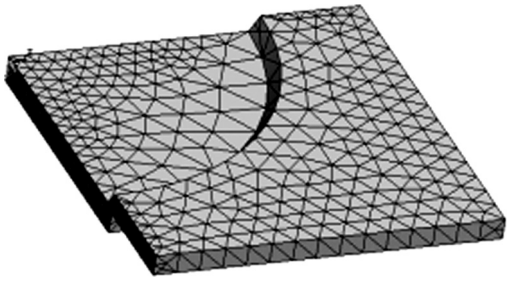

Fig. 4. FEM model of one-fourth part of the transducer

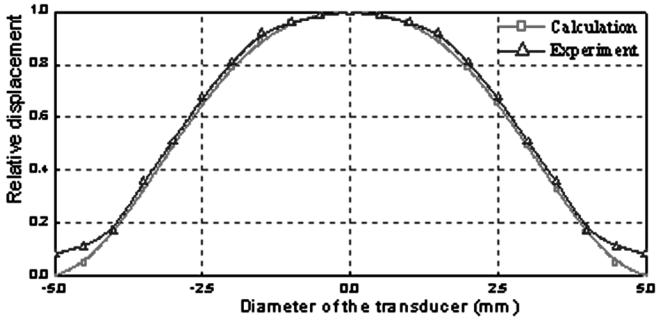

Fig. 5. The first mode shape curve of the transducer

one. The reason is that the calculation model of the transducer just considered the chamber part of the device. Compared to the real device, the calculation model has a bigger rigidity, which results in a higher calculated frequency. The real boundary conditions are that the rims around the elastic plate, not the edge of the chamber, are clamped, which results in the difference of the mode shape near the chamber edge. We also simulated the same structure as the calculation model and got the first mode frequency of 36.8 kHz, which is almost equal to the calculated frequency. Although there are some differences between the calculated and measured results, the approximate calculation is simple and useful for primary design of the transducer.

4.2
Comparison of axisymmetric vibration modes

For some piezoelectric transducers working at higher frequencies, in addition to the first mode more higher order vibration modes are needed to evaluate the stability and efficiency of the working status. FEM has been introduced for higher modal analysis of the transducers. However, experiments to measure the vibration modes are still necessary to validate the simulation model.

In this paper, a scanning laser Doppler vibrometers (SLDV), Polytec's PSV-300, has been employed to measure the transducer. This non-contacting measurement instrument has a 0.5–250 kHz band width with 0.3 μm/s accuracy, which can meet the experimental requirements. In the experiment, the four rims of the elastic plate are clamped, and due to the larger thickness of the rims, resulting in less amplitude at these areas, only the chamber membrane is measured with 300 scanning points.

Figure 6b illustrates the three preceding axisymmetric vibration modes of the transducer corresponding to resonant frequencies at 28.1, 52.8 and 144.2 kHz. Not all modes are equally strong present. Due to a finite quality factor (Q-factor), some modes appear simultaneously. Especially for higher vibration modes, the mixing of modes is more obvious and serious. That is why in the experiment, it's hard to obtain steady plots for further higher vibration modes. For the functioning of the device, only the modes that are strongly and clearly separated from the others are of interest.

Comparing the simulation results with the experimental results as shown in Fig. 6, the resonant frequencies obtained by measurement are a little bit larger than the simulation results, and the higher vibration mode shapes are almost the same. Generally, geometrical differences and the real boundary conditions, not as rigid as that in the calculation, are the major factors resulting in basic differences between the calculated resonance frequencies and reality. By adjusting the stiffness of the boundaries, simulation results more coinciding to the experimental results have been obtained. When the outer rims with the width of 1 mm of the square structure are clamped, the first mode frequency is about 28.4 kHz, quite close to the experimental result.

5
Conclusions

In this paper, an approximate method has been introduced to evaluate the basic vibration mode and FEM has been used to simulate the higher order vibration modes of the transducer. Comparisons with the experimental results have proved the validation of the models. Therefore, these

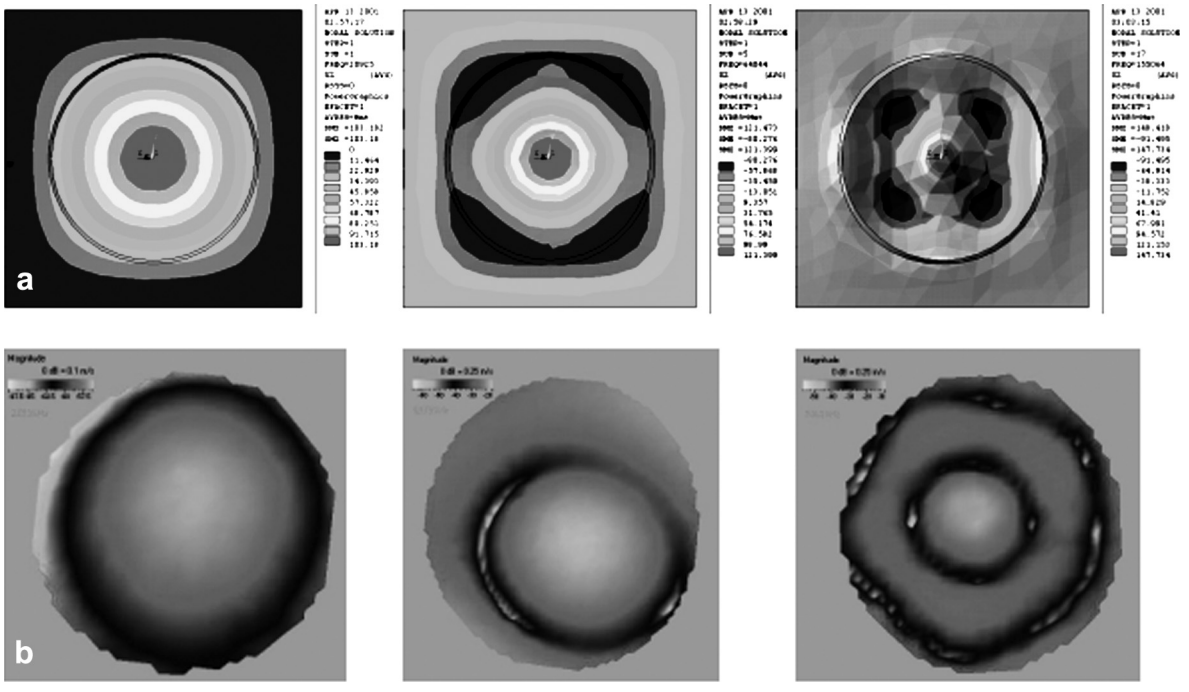

Fig. 6a, b. The comparison of simulation results to experimental results of the first three axisymmetric modes of the transducer. **a** Simulation results of the first three modes (f =21, 64 and 155 kHz); **b** experimental results of the first three modes (f =28.1, 52.8 and 144.2 kHz)

two methods can be employed to optimize the design of piezoelectric transducers, to analyze the characteristics of the transducers and to predict the working status of the devices.

References

1. **Van Lintel H** (1988) A piezoelectric micropump based on micromachined of silicon. Sensors and Actuators 15: 153–167
2. **Percin G; Levin L.; Khuri-Yakub, BT** (1996) Piezoelectrically actuated transducer and droplet ejector. In: IEEE Ultrasonics Symposium, pp 913–916
3. **Luginbuhl Ph; Indermuhle P; Gretillat M;** et al (1999) Micromachined injector for DNA mass spectrometry. In: Proceedings of the Transducers'99. Sendai, Japan, pp 1130–1133
4. **de Heij B; van der Schoot B; Bo H.;** et al. (2000) Characterisation of a fL droplet generator for inhalation drug therapy. Sensor and Actuators A85 (3): 430–434
5. **Liu C; Zhou Z; Wang X; Xiong J** (2001) A piezoelectrically actuated microjet. In: 4th International Symposium on Test & Measurement. Shanghai, China
6. **Hwang W; Park HC** (1992) Finite element modeling of piezoelectric sensors and actuators. AIAA J 30(3): 930–937
7. **de Heij B; van der Schoot B; de Rooij NF** et al. (1999) Modelling and optimization of a vaporizer for inhalation drug therapy. In: Technical Proceedings of the Second International Conference on Modelling and Simulation of Microsystems, pp 542–545
8. **Wang Q.-M.; Du X-H; Xu B; Eric Cross L** (1999) Electromechanical coupling and output efficiency of piezoelectric bending actuators. IEEE Transactions on Ultrasonics, Ferroelectrics, and Frequency control 46(3): 638–646
9. **Ikeda T** (1990) Fundamentals of piezoelectricity. Oxford, New York